# European Journal of Chemistry

Journal webpage: www.eurjchem.com

# Nanostructured thin film of iron tin oxide by aerosol assisted chemical vapour deposition using a new ferrocene containing heterobimetallic complex as single-source precursor

Sohail Saeed [1,2,*], Nasir Khan [3], Ray Butcher [4] and Naghmana Rashid [5]

[1] National Engineering and Scientific Commission, Islamabad, 45320, Pakistan
[2] Department of Chemistry and School of Materials Science, University of Manchester, Oxford Road, Manchester M35 9PL, United Kingdom
[3] Department of Chemistry, Quaid-i-Azam University, Islamabad, 45320, Pakistan
[4] Chemistry Department, Howard University, Washington, DC 20059, USA
[5] Department of Chemistry, Research Complex, Allama Iqbal Open University, Islamabad, 45320, Pakistan

* Corresponding author at: National Engineering and Scientific Commission, Islamabad, 45320, Pakistan.
Tel.: +92.51.90133246. Fax: +92.51.90133685. E-mail address: sohail262001@yahoo.com (S. Saeed).

## ARTICLE INFORMATION

## ABSTRACT

Aerosol assisted chemical vapour deposition (CVD) is a sophisticated, unique and modern technique which is used to deposit coatings, films, and other related structures from thermally unstable or the involatile precursors at laboratory and large scale productions. A light weight semiconducting and ceramic oxide based coatings on appropriate substrates can be produced at a lower cost by employing chemical vapour deposition method. There is broader choice of chemical precursors and their availability for obtaining high quality thin films at lower cost and the reaction environment is more flexible ranging from low pressure to atmospheric pressure in CVD. New ferrocene containingheterobimetallic precursor, $[C_{58}H_{80}Fe_2O_4Sn_2]$ has been synthesized and characterized by elemental analysis, FT-IR spectroscopy, thermogravimetric analysis and molecular structure was determined by X-ray single crystal analysis. The heterobimetallic complex was used as a single-source precursor for the growth of iron tin oxide thin film by aerosol assisted chemical vapor deposition. The deposited thin film was characterized by X-ray diffractometer, scanning electron microscopy and atomic force microscopy techniques. The average roughness of deposited film at 425 °C from heterobimetallic precursor was in the range of 4.39 nm. The deposited thin film on glass strip was found to have no cracks, excellent adhesion and to be crystalline in nature and free from any carbonaceous impurities.

Cite this: Eur. J. Chem. 2017, 8(3), 224-228

## 1. Introduction

Nanostructured thin films of ceramic oxides are finding ever-increasing applications in advanced nanomaterial technology due to their modified surface morphologies [1]. Tin oxide is an *n*-type semiconductor with a band gap, $E_{gap}$, of 3.6 eV at 27 °C [2]. Being a semiconducting nature of tin oxide, it has numerous applications in transistors [3], solar cells [4] and as a gas sensor [5] by virtue of its chemical durability, thermal stability, and non-stoichiometric stable phases [6]. Certain limitations e.g. cross sensitivity [7], and high operation temperature for gas sensing [8] have been observed for tin oxide gas sensors. These disadvantages may be fixed by modifying the adsorption surface sites of these sensors [9]. Those metals whose electronegativity is lower than Sn(IV) have outstanding sensitivity when doped into tin oxide [10]. Doping of tin oxide with noble metals (Palladium, Platinum, Gold) and other metals (Fe, Co, Ni, Mn, Sb and Zn) [11] has been extensively studied [12]. The incorporation of iron into tin oxide reduces the amount of oxygen bonded to tin, which in turn enhances the sensing ability of tin [13]. These exceptional properties of iron oxides, coupled with a large surface-to-volume ratio of tin oxide, results in high selectivity and sensitivity in these composite materials [2]. Tin oxide doping with magnetite ($Fe_3O_4$), maghemite ($\gamma$-$Fe_2O_3$) and hematite ($\alpha$-$Fe_2O_3$) have been reported to manifest efficient gas sensing properties [14]. Gas sensors made from these hybrid composite materials by doping method have a lower operating temperature and sensitivity due to an enhanced surface-to-volume ratio [15]. Structural changes associated with doping mainly depend on the method of synthesis of these composite materials [16]. Iron doped tin oxides have been reported using different techniques, viz. the sol-gel technique [17], pulsed laser pyrolysis deposition, co-precipitation [18], solvothermal reduction [19], ball milling [20], combustion [21], and atomic layer deposition [22]. The usefulness of heterobimetallic coordination complexes as single source precursors for the formation of mixed-metal oxides thin films is relatively less explored [23].
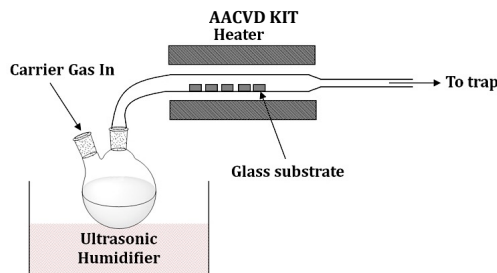
**Figure 1.** Schematic diagram of an aerosol assisted chemical vapour deposition (AACVD) arrangement.

Herein, we report the syntheses of a novel ferrocene containing bimetallic complex [$C_{58}H_{80}Fe_2O_4Sn_2$] and it was used in the fabrication of iron tin oxide thin film using CVD.

## 2. Experimental

### 2.1. Materials and physical measurements

All the synthetic work was carried out under an inert atmosphere of dry nitrogen using standard Schlenk techniques. All the chemicals were purchased from Sigma-Aldrich and used as received. Elemental analysis was performed by the University of Manchester micro-analytical laboratory. Infrared spectra were recorded on a Specac single reflectance Attenuated Total Reflectance (ATR) instrument (4000-400 cm$^{-1}$, resolution 4 cm$^{-1}$). TGA measurements were carried out by a Seiko SSC/S200 model under a heating rate of 10 °C/min under nitrogen. p-XRD studies were performed on a Bruker AXSD8 diffractometer using CuKα radiation. Scanning electron microscopy (SEM) analysis was performed using a Philips XL 30FEG. Single crystal X-ray diffraction data for hetero-bimetallic complex was collected using graphite-monochromated MoKα radiation (λ = 0.71073 Å) on a Bruker SMART 1000 CCD diffractometer.

### 2.2. Synthesis of heterobimetallic single-source precursor

4-Ferrocenyl benzoic acid (6.2 g, 20 mmol) was added to a 500 mL round bottom flask charged with tributyltin chloride (6.50 g, 20 mmol) and triethyl amine (2.8 mL, 20 mmol) in 100 mL dry toluene with constant stirring and refluxed for 10 hrs. The mixture was cooled to room temperature, filtered and the filtrate was vacuum evaporated. Product was re-crystallized from ethanol as orange red crystals. Yield: 81%. M.p: 76-78 °C. Anal. calcd. for $C_{58}H_{80}Fe_2O_4Sn_2$: C, 58.52; H, 6.72. Found: C, 58.37; H, 6.76%. FT-IR (ATR, ν, cm$^{-1}$): 3087w, 2952m, 2917m, 2868m, 2853m, 1582s (COO$_{sym}$), 1357s (COO$_{asym}$), 471s (Sn-C), 429 m (Sn-O). TGA (Temp., °C (%)): 102-226 (12.5), 229-285 (18.1), 285-329 (21.5), 355-517 (9.5), residue 453-552 (38.3).

### 2.3. Deposition of iron tin oxide thin films by aerosol assisted chemical vapour deposition (AACVD)

Experiment for the deposition of iron tin oxide thin film by AACVD was designed according to the experimental setups of Saeed and co-workers [24-30]. In a typical deposition, 0.25 g of the precursor was dissolved in 15 mL THF in a two-necked 100 mL round-bottom flask with a gas inlet that allowed the carrier gas (argon) to pass into the solution to aid the transport of the aerosol (Figure 1). This flask was connected to the reactor tube by a piece of reinforced tubing. The argon flow rate was controlled by a Platon flow gauge. Seven soda glass substrates (approx. 1 × 2 cm) were placed inside the reactor tube, which is placed in a CARBOLITE furnace. The precursor solution in a round-bottom flask was kept in a water

bath above the piezoelectric modulator of a PIFCO ultrasonic humidifier (Model No. 1077). The aerosol droplets of the precursor thus generated were transferred into the hot wall zone of the reactor by carrier gas. Both the solvent and the precursor were evaporated and the precursor vapour reached the heated substrate surface where thermally induced reactions and film deposition took place.

## 3. Results and discussion

### 3.1. Spectroscopic characterization

The bimetallic compound was crystallized from ethanol. The ferrocenyl carboxylate showed mono and bidentate coordination modes with the organotin(IV) derivatives. The newly synthesized ferrocene containing compound was also found to be air and water stable. In the IR spectra, the disappearance of the characteristic peak in the region 3500-3300 cm$^{-1}$ for the hydroxy moiety of the carboxylic acid indicates deprotonation and constitution of organotin(IV) derivative. The carboxylic functional group, tin-carbon linkage, tin-oxygen linkage, and tin-oxygen-tin linkage vibrational frequencies present the valuable and direct information about geometry around the tin center [31-33]. The typical carboxylic group absorption bands for the compound exhibit υCOO$_{as}$ and υCOO$_s$ stretching frequencies in regions 1595 and 1357 cm$^{-1}$ respectively. The stretching frequency difference (COO$_{as}$-COO$_s$) was found to be 238 cm$^{-1}$, which is the indication of bridging behavior in the bimetallic structure. The stretching frequency at 685 cm$^{-1}$ in the spectra of the complex is due to tin-oxygen-tin bonding which is also supporting the bridging behavior.

### 3.2. Single crystal X-ray crystallography

The molecular structure and unit cell diagrams of $C_{58}H_{80}Fe_2O_4Sn_2$ are shown in Figure 2 and 3, respectively; crystal data and refinement and selected bond lengths and angles are listed in Table 1 and 2, respectively.

The polymeric nature and *trans*-O$_2$SnC$_3$-coordination sphere is common for R$_3$SnO$_2$CR' (where R = *n*-alkyl groups) [34]. The nature of the bridging is anisotropic, in which tin forms one short [Sn(1)-O(1) 215.5(4) pm] and one relatively long [Sn(1)-O(2) 255.6(4) pm] bond to oxygen. These bond lengths are comparable to other Sn-O bonds found in typical polymeric triorganotin carboxylates, with short (212.0-224.6 pm) and long (224-265 pm) bonds, respectively. The O(1)-Sn(1)-O(2) angle [167.5(8)°] is also comparable to other angles found in typical polymeric triorganotin carboxylates (168.6-178.7°) [35]. The ferrocene unit is attached on the one dimensional zig-zag polymeric structure and is directed up and downwards, alternative to the tin carboxylate plane. This setup is unique in a sense that it is a heterobimetallic metal organic network in which one metal atom (Sn) contributes to the bonding for the formation of the network structure and the other metal atom (Fe) is just attached to the polymeric structure as a branch.

**Table 1.** Crystal data and structure refinement for heterobimetallic complex.

| | |
|---|---|
| CCDC | 907720 |
| Empirical formula | $C_{58}H_{80}Fe_2O_4Sn_2$ |
| Formula weight | 1190.30 |
| Temperature | 123(2) K |
| Wavelength | 1.54184 Å |
| Crystal system | Monoclinic |
| Space group | C 2/c |
| Unit cell dimensions | a = 24.4783(8) Å |
| | b = 10.6447(3) Å |
| | c = 22.2712(8) Å |
| | β = 111.939(4)°. |
| Volume | 5382.8(3) Å³ |
| Z | 4 |
| Density (calculated) | 1.469 Mg/m³ |
| Absorption coefficient | 11.866 mm⁻¹ |
| F(000) | 2448 |
| Crystal size | 0.7098 × 0.2650 × 0.0892 mm³ |
| Theta range for data collection | 4.28 to 75.76°. |
| Index ranges | -29 ≤ h ≤ 30, -13 ≤ k ≤ 10, -27 ≤ l ≤ 27 |
| Reflections collected | 18263 |
| Independent reflections | 5507 [R(int) = 0.0508] |
| Completeness to theta = 67.50° | 99.5 % |
| Absorption correction | Analytical |
| Max. and min. transmission | 0.446 and 0.063 |
| Refinement method | Full-matrix least-squares on $F^2$ |
| Data / restraints / parameters | 5507 / 155 / 387 |
| Goodness-of-fit on $F^2$ | 1.023 |
| Final R indices [I>2sigma(I)] | R1 = 0.0474, wR2 = 0.1244 |
| R indices (all data) | R1 = 0.0557, wR2 = 0.1308 |
| Extinction coefficient | 0.000028(11) |
| Largest diff. peak and hole | 1.635 and -0.984 e.Å⁻³ |

**Table 2.** Bond lengths [Å], bond angles [°] and torsion angles [°] for hetero-bimetallic complex.

| **Bond lengths [Å]** | |
|---|---|
| Sn-C(1C) | 2.010(4) |
| Sn-C(1B) | 2.048(11) |
| Sn-C(1BC) | 2.144(11) |
| Sn-C(1A) | 2.148(3) |
| Sn-O(2) | 2.1939(19) |
| Sn-C(1BA) | 2.252(17) |
| Sn-C(1CA) | 2.325(7) |
| Sn-O(1)#1 | 2.450(2) |
| Fe-C(13) | 2.041(3) |
| Fe-C(12) | 2.042(3) |
| **Bond angles [°]** | |
| C(1BC)-Sn-O(2) | 96.2(3) |
| C(1A)-Sn-O(2) | 89.08(10) |
| C(1C)-Sn-C(1BA) | 119.2(4) |
| C(1B)-Sn-C(1BA) | 4.4(5) |
| C(1BC)-Sn-C(1BA) | 3.7(4) |
| C(1A)-Sn-C(1BA) | 117.1(4) |
| O(2)-Sn-C(1BA) | 98.8(4) |
| C(1C)-Sn-C(1CA) | 1.5(3) |
| C(1B)-Sn-C(1CA) | 118.0(3) |
| C(1BC)-Sn-C(1CA) | 118.4(3) |
| C(1A)-Sn-C(1CA) | 120.6(2) |
| C(13)-Fe-C(12) | 159.01(15) |
| C(13)-Fe-C(17) | 40.53(14) |
| C(12)-Fe-C(17) | 122.91(14) |
| C(13)-Fe-C(10) | 122.46(13) |
| C(12)-Fe-C(10) | 68.32(13) |
| C(17)-Fe-C(10) | 157.52(13) |
| C(13)-Fe-C(11) | 158.36(15) |
| C(12)-Fe-C(11) | 40.93(14) |
| **Torsion angles [°]** | |
| C(1C)-Sn-O(2)-C(1) | 71.4(3) |
| C(1B)-Sn-O(2)-C(1) | -47.7(3) |
| C(1BC)-Sn-O(2)-C(1) | -46.8(3) |
| C(1A)-Sn-O(2)-C(1) | -166.8(3) |
| C(1BA)-Sn-O(2)-C(1) | -49.5(4) |
| C(1CA)-Sn-O(2)-C(1) | 72.6(3) |
| O(1)#1-Sn-O(2)-C(1) | 175.4(3) |
| Sn#2-O(1)-C(1)-O(2) | -157.8(3) |
| Sn#2-O(1)-C(1)-C(2) | 19.7(6) |
| Sn-O(2)-C(1)-O(1) | -0.8(4) |
| Sn-O(2)-C(1)-C(2) | -178.46(17) |
| C(10)-Fe-C(8)-C(12) | 81.3(2) |
| C(11)-Fe-C(8)-C(12) | 37.78(19) |
| C(16)-Fe-C(8)-C(12) | -79.8(2) |
| C(15)-Fe-C(8)-C(12) | -48.2(5) |

Symmetry codes: #1= 1/2-*x*, 1/2+*y*, 3/2-*z*, #2= 1/2-*x*, -1/2+*y*, 3/2-*z*.
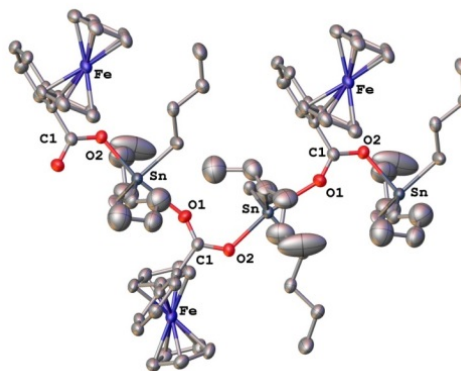


**Figure 2.** The ORTEP plot of the heterobimetallic complex was shown at 50% probability thermal ellipsoids.
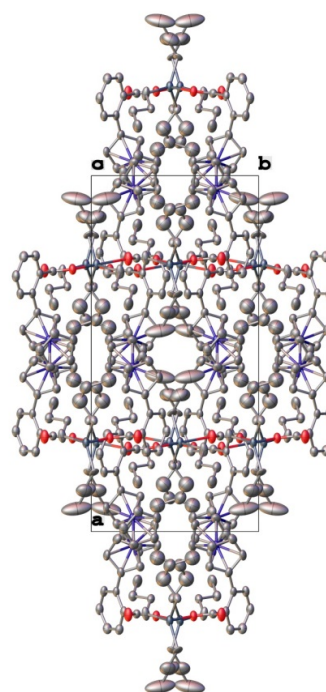


**Figure 3.** Packing diagram of heterobimetallic complex along *c*-axis ($C_{58}H_{80}Fe_2O_4Sn_2$).

### 3.3. Thermal decomposition studies of heterobimetallic complex by TGA

TGA of the heterobimetallic complex indicates four stages of weight loss. In the first step decomposition starts at 102 °C and completes at 226 °C with weight loss of 12.5% which is equivalent to the weight of the butyl group ($-C_4H_9$). The second decomposition step starts at 229 °C and completes at 285 °C, with weight loss of 18.1% corresponding to the aromatic group. The third decomposition stage starts at 286 °C and ends at 329.3 °C, with an endothermic weight loss of the cyclopentadienyl ($-C_5H_6$) fragment. The last decomposition step occurs at 355-517 °C, corresponding to the evolution of CO from a carboxylate group with a weight loss of 9.5% and leaving a residue of 38.3% of the initial weight. This residual weight is almost close to the expected composition for $SnO_2.0.5Fe_2O_3$ (38%). This composition is also in agreement with the p-XRD phase identification results.

### *3.4. Crystlline phases and stoichiometry identification by XRD studies*

Based on the thermogravimetric analysis data, the AACVD experiment for precursor was run at 425 °C with an argon flow rate at of 160 sccm on glass substrates. Dark black adherent uniform film was deposited at 425 °C. The X-ray diffraction pattern of as deposited film at 425 °C from precursor is shown in Figure 4.
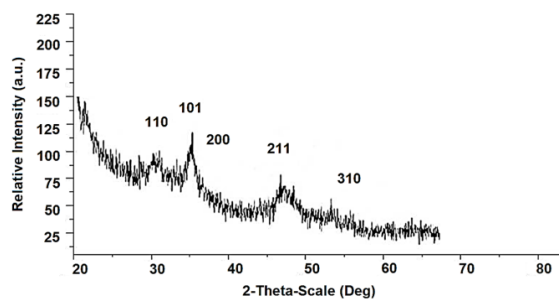


**Figure 4.** p-XRD pattern of oxide acquired from precursor.

The thin film developed at 425 °C produced three broad Braggs peak at 26.6, 33.9 and 51.8°, and three other peaks at 54.7, 61.8 and 71.2°, indexed as cassiterite syn (ICDD 04-003-0974) [36], having a tetragonal system with the P42mnm (136) space group. The lattice dimensions a = b = 4.738 Å and c = 3.186 Å and no peak for iron oxide were observed; the decrease in the crystallite size and broadening of the peak suggests that the iron has become incorporated in the tin oxide lattice [37] due to small difference between the atomic radii of tin (0.71 nm) and iron (0.68 nm) without effecting the lattice, on the other hand iron also acts as crystallite inhibitor for tin dioxide. Thus iron can amalgamate, which increases the stacking fault density of tin dioxide.

### *3.5. Scanning electron microscopic and atomic force microscopic studies*

The surface morphology of the deposited film at 425 °C was studied using scanning electron microscopy; the microgram (Figure 5) revealed that the film was composed of irregular dispersed flowering globules.
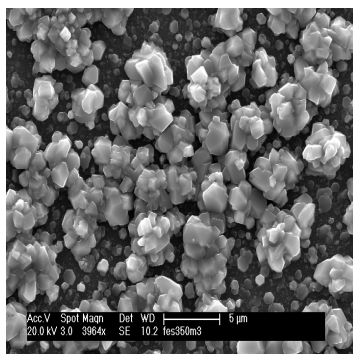


**Figure 5.** SEM image of the thin film deposited from heterobimetallic complex at 425 °C.

The irregular shape of the particles can be attributed to iron doping into the tin oxide lattice. The literature shows that iron acts as a crystallite inhibitor [38]. The AFM micrographs (Figure 6a and 6b) for the surface topology of the deposited film at 425 °C show non-homogeneously dispersed surfaces throughout the film. The thickness of the film and crystallite size is controlled by the optimization time of deposition and concentration of precursor solution [39]. The AFM image of the thin film shows the growth of closely packed crystallites onto a glass substrate with an average roughness of 4.39 nm.
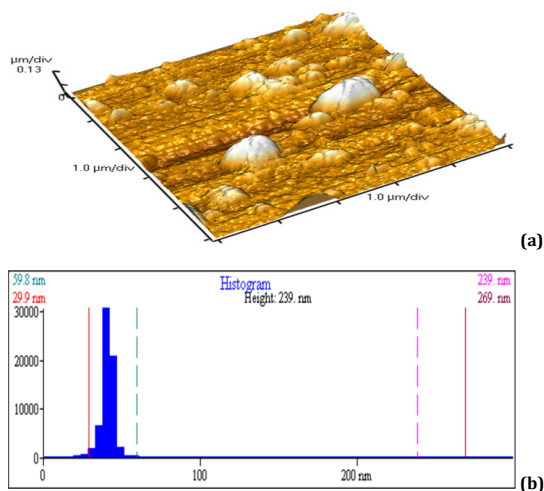


| Region | Rp-v, nm | Rms rough (Rq), nm | Ave rough (Ra), nm | Mean Ht, nm | Median Ht, nm |
|--------|----------|--------------------|--------------------|-------------|---------------|
| 1 | 298.8 | 13.50 | 4.393 | 41.81 | 40.99 |

**Figure 6.** (**a**) AFM image in 3D view of film deposited at 425 °C; (**b**) Histogram of thin film deposited at 425 °C showing average roughness and RMS roughness morphology.

### 4. Conclusions

The newly synthesized ferrocene containing hetero-bimetallic complex was used for the growth of nanostructured thin film of iron tin oxide by aerosol-assisted chemical vapor deposition. The average roughness of deposited film from ferrocene containing heterobimetallic complex was in the range of 4.39 nm. The precursor shows the cassititrite phase of tin with iron incorporation in the lattice. The optimized conditions for the deposition of iron tin oxide thin film from heterobimetallic precursor by AACVD may be used for the manufacturing of solar cells and gas sensors.

### Supplementary crystallographic data

CCDC-907720 is the reference number of crystallographic data for the heterobimetallic complex structure reported in this article. It has been deposited with Cambridge Crystallographic Data Centre. Soft copies of the complete detail of crystallographic data of the said structure may be obtained free of charge from the Director, CCDC, 12 Union Road, Cambridge, CBZ IEZ, UK. Facsimile (44) 01223 336 033, E-mail: deposit@ccdc.cam.ac.uk or http://www.ccdc.com.ac.uk/deposit.

### References

[1]. Brown, K. R.; Fox, A. P.; Natan, M. J. *J. Am. Chem. Soc.* **1996**, *118(5)*, 1154-1157.

[2].  Kormunda, M.; Pavlik, J. *Vacuum* **2011**, *85(9)*, 871-874.
[3].  Sun, J.; Liu, H.; Jiang, J.; Lu, A.; Wan, Q. *J. Mater. Chem.* **2010**, *20(37)*, 8010-8015.
[4].  Gubbala, S.; Chakrapani, V.; Kumar, V.; Sunkara, M. K. *Adv. Funct. Mater.* **2008**, *18(16)*, 2411-2418.
[5].  Wang, B.; Zhu, L.; Yang, Y.; Xu, N.; Yang, G. *J. Phys. Chem. C* **2008**, *112 (17)*, 6643-6647.
[6].  Kida, T.; Doi, T.; Shimanoe, K. *Chem. Mater.* **2010**, *22(8)*, 2662-2667.
[7].  Sarala-Devi, G.; Manorama, S.; Rao, V. *Sens. Actuators B: Chem.* **1995**, *28(1),* 31-37.
[8].  Pan, J.; Ganesan, R.; Shen, H.; Mathur, S. *J. Phys. Chem. C* **2010**, *114(18),* 8245-8250.
[9].  Deskins, N. A.; Rousseau, R.; Dupuis, M. *J. Phys. Chem. C* **2010**, *114(13),* 5891-5897.
[10].  Yamazoe, N. *Sen. Actuators B: Chem.* **1991**, *5(1-4),* 7-19.
[11].  Rani, S.; Roy, S. C.; Bhatnagar, M. *Sens. Actuators B: Chem.* **2007**, *122(1),* 204-210.
[12].  Siciliano, P. *Sens. Actuators B: Chem.* **2000**, *70(1-3),* 153-164.
[13].  Mehraj, S. *Sci. Adv. Mater.* **2012**, *4(12),* 1258-1267.
[14].  Liao, M. H.; Chen, D. H. *J. Mater. Chem.* **2002**, *12*, 3654-3659.
[15].  Jing, Z.; Wu, S. *Mater. Lett.* **2006**, *60(7)*, 952-956.
[16].  Stambolova, I.; Blaskov, V.; Vassilev, S.; Shipochka, M.; Dushkin, C. *J. Alloy Compd.* **2010**, *489(1)*, 257-261.
[17].  Yang, B.; Li, Z.; Gao, Y.; Lin, Y.; Nan, C. -W. *J. Alloy Compd.* **2011**, *509(13)*, 4608-4612.
[18].  Alexandrescu, R.; Morjan, I.; Dumitrache, F.; Birjega, R.; Fleaca, C.; Soare, I.; Gavrila, L.; Luculescu, C.; Prodan, G.; Kuncser, V.; Filoti, G. *Appl. Surf. Sci.* **2011**, *257(12)*, 5460-5464.
[19].  Altincekic, T. G.; Boz, I.; Baykal, A.; Kazan, S.; Topkaya, R.; Toprak, M. S. *J. Alloy Compd.* **2010**, *493(1-2)*, 493-498.
[20].  Goya, G. F.; Rechenberg, H. R. *Nanostruct. Mater.* **1998**, *10(6)*, 1001-1011.
[21].  Zhang, Y.; Stangle, G. C. *J. Mater. Res.* **1994**, *9(8)*, 1997-2004.
[22].  Tamm, A.; Dimri, M. C.; Kozlova, J.; Aidla, A.; Tätte, T.; Arroval, T.; Mäeorg, U.; Mändar, H.; Stern, R.; Kukli, K. *J. Cryst. Growth*, **2012**, 343(1), 21-27.
[23].  Veith, M. *J. Chem. Soc. Dalton Trans.* **2002**, *12*, 2405-2412.
[24].  Saeed, S.; Rashid, N.; Malik, M. A.; O'Brien, P.; Wong, W. T. *New J. Chem.* **2013**, *37(10)*, 3214-3221.
[25].  Saeed, S.; Rashid, N.; Malik, M. A.; O'Brien, P.; Wong, W. T. *J. Coord. Chem.* **2013**, *66(16)*, 2788-2801.
[26].  Saeed, S.; Rashid, N.; Ahmad, K. S. *Turk J. Chem.* **2013**, *37(5)*, 796-804.
[27].  Saeed, S.; Hussain, R.; Butcher, R. J. *J. Coord. Chem.* **2014**, *67(10)*, 1693-1701.
[28].  Saeed, S.; Hussain, R. *J. Coord. Chem.* **2014**, *67(17)*, 2942-2953.
[29].  Saeed, S.; Hussain, R. *Turk J. Chem.* **2014**, *38(3)*, 413-422.
[30].  Saeed, S.; Ahmad, K. S.; Rashid, N.; Malik, M. A.; O'Brien, P.; Akhtar, M.; Hussain, R.; Wong, W. T. *Polyhedron* **2015**, *85*, 267-274.
[31].  Lal, B.; Badshah, A.; Altaf, A. A.; Khan, N.; Ullah, S. *Appl. Organomet. Chem.* **2011**, *25(12)*, 843-855.
[32].  Lal, B.; Badshah, A.; Altaf, A. A.; Tahir, M. N.; Ullah, S.; Huq, F. *Dalton Trans.* **2012**, *41(48)*, 14643-14650.
[33].  Khan, N.; Badshah, A.; Lal, B.; Malik, M. A.; Raftery, J.; O'Brien, P.; Altaf, A. A. *Polyhedron* **2014**, *69*, 40-47.
[34].  Mahon, M. F.; Molloy, K. C.; Stanley, J. E.; Rankin, D. W. H.; Robertson, H. E.; Johnston, B. F. *Appl. Organome. Chem.* **2005**, *19(5)*, 658-671.
[35].  Tiekink, E. R. T. *Trend Organomet. Chem.* **1994**, *1(1)*, 71-116.
[36].  Baur, W. H.; Khan, A. A. *Acta Crystallogr. Sect. B* **1971**, *27*, 2133-2139.
[37].  Knapp, C. E.; Hyett, G.; Parkin, I. P.; Carmalt, C. J. *Chem. Mater.* **2011**, *23(7)*, 1719-1726.
[38].  Castro, R. H. R.; Hidalgo, P.; Muccillo, R. Gouvea, D. *Appl. Surf. Sci.* **2003**, *214(1-4)*, 172-177.
[39].  Barnes, T. M.; Hand, S.; Leaf, J.; Wolden, C. A. *J. Vac. Sci. Technol.* **2004**, *22(5)*, 2118-2125.